Assembling nanoscale zero-valent iron on magnetic Fe$_3$O$_4$/reduced graphene oxide composite for efficient reduction of hexanitrohexaazaisowurtzitane (CL-20)

Dejin Zhang[†], Yinglu Sun[†], Xinbai Jiang*, Xiaodong Liu, Xiuyun Sun, Jiansheng Li, Weiqing Han, Lianjun Wang, Jinyou Shen*

Jiangsu Key Laboratory of Chemical Pollution Control and Resources Reuse, School of Environmental and Biological Engineering, Nanjing University of Science and Technology, Nanjing 210094, China, emails: xinbai_jiang@mail.njust.edu.cn (X. Jiang), shenjinyou@mail.njust.edu.cn (J. Shen), zhdj92@163.com (D. Zhang), 513305365@qq.com (Y. Sun), liuxd@mail.njust.edu.cn (X. Liu), sunxyun@njust.edu.cn (X. Sun), lijsh@njust.edu.cn (J. Li), hwqnjust@aliyun.com (W. Han), wanglj@njust.edu.cn (L. Wang)

ABSTRACT

To increase the hexanitrohexaazaisowurtzitane (CL-20) removal capacity of nanoscale zero-valent iron (nZVI), the present study explored a facile modification route based on the assembling of nZVI onto a magnetic Fe$_3$O$_4$/reduced graphene oxide (MG) composite. These nZVI particles were well dispersed and tightly attached on the basal plane of reduced graphene oxide (rGO) with Fe$_3$O$_4$ integration as the middle layer. These nZVI@MG composites showed better CL-20 removal efficiency, compared with commercial ZVI, nZVI, MG and nZVI assembled on rGO (nZVI@rGO). The rGO and Fe$_3$O$_4$ played a confirming role in alleviating the agglomeration and improving nZVI reducibility. The CL-20 removal process by nZVI@MG followed a pseudo-second-order kinetics model, indicating the involvement of hybrid adsorption and chemical reactions. Three intermediates during CL-20 reduction by nZVI@MG were identified through LC-MS or GC-MS. Based on these intermediates, two distinct pathways were proposed. This study demonstrated that nZVI@MG composites could be promisingly implemented as an environmentally friendly and inexpensive material for CL-20 removal from wastewater.

Keywords: Hexanitrohexaazaisowurtzitane; Nanoscale zero-valent iron; Magnetic Fe$_3$O$_4$; Reduced graphene oxide; Reduction

1. Introduction

Hexanitrohexaazaisowurtzitane (CL-20) is a newly developed energetic material, which shows higher energy density than currently used cyclic-nitramine explosives such as cyclotetramethylenetetranitramine and cyclotrimethylenetrinitramine. CL-20 is expected to replace these energetic materials, which are currently widely used [1,2]. Therefore, development and manufacture of CL-20 for a wider military and industrial application is currently essential. Considering the fact that CL-20 is highly toxic to various organisms, such

as *Eisenia andrei* [3], *Enchytraeus crypticus* and *Enchytraeus albidus* [4,5], the manufacture and usage of CL-20 would result in severe contamination of both soil and water supplies [6]. In the future, with the wider application of CL-20, environmental remediation of CL-20 pollution will become a rather important topic.

Various technologies, such as biodegradation, alkaline hydrolysis and photolysis have been developed for CL-20 removal from contaminated soil and wastewater. Trott et al. [7] have found that 80% of CL-20 can be degraded in garden soil after a 2-d incubation. A CL-20-degrading bacterial

---

strain, *Agrobacterium* sp. strain JS71, has been isolated from an enriched culture, using garden soil as the inocula. However, the requirement of an additional carbon source such as succinate, and the difficulty in CL-20 mineralization limits the application of biodegradation technology. Alkaline hydrolysis has been suggested to be a promising alternative for CL-20 degradation. Karakaya et al. [8] have indicated that the structure of CL-20 is effectively hydrolyzed within a OH^- concentration range from 0.25 to 300 mM. Balakrishnan et al. [9] have investigated the alkaline hydrolysis of CL-20, showing that the initial denitration of CL-20 in water is sufficient to cause ring cleavage, followed by spontaneous decomposition to form final products. However, much alkaline chemical is consumed, resulting in the substantial increase in salt content in the treated effluent, which is unfavorable for the subsequent biodegradation process. Hawari et al. [10] have investigated the photolysis of CL-20 in a Rayonet photoreactor using sunlight as the light source, with NO_2^-, NO_3^-, NH_3, HCOOH, N_2 and N_2O observed as photolytic products. However, for CL-20 photolysis, it has been suggested that photocatalytic degradation shows a high dependence on available light and electrical energy. Therefore, it is particularly urgent to develop an efficient and low-energy consumption method for CL-20 removal from wastewater.

Reduction of various nitroaromatic compounds, such as CL-20, by zero-valent iron (ZVI) has turned out to be a potential and economical method. Balakrishnan et al. [11] have explored the decomposition of CL-20 by ZVI powder and found that CL-20 degradation in water leads to the formation of nitrous oxide, ammonium and formate. However, ZVI powder dosage as high as 10 g/L is required to completely remove 100 mg/L CL-20. The poor reduction efficiency of CL-20 by ZVI has been attributed to the limited reactive sites of ZVI powder and poor mass transfer between ZVI powder and CL-20, which needs to be improved. Nanoscale zero-valent iron (nZVI) particles are gaining increasing attention because of its significant specific surface area, permeability and reactivity arising from its extremely small particle size [12,13]. However, bare nZVI particles are unstable in water, and exhibit a high tendency to agglomerate due to the magnetic and gravitational forces and high interfacial energy [14,15]. Both passivation shell and agglomeration result in a dramatic decline in the function of nZVI, limiting the scaled application in wastewater treatment. Many efforts has been devoted to mitigating or eliminating the passivation and agglomeration of nZVI, including such strategies as modification of nZVI surfaces and nZVI support onto granular particles [16,17]. Providing an external supporter seems to be an effective, recyclable and environmentally friendly approach. Various supporters, including active carbon [18], multiwalled carbon nanotubes [19], resin [20] and bentonite [21], have been successfully used for nZVI loading.

Graphene, a one atom-thick two-dimensional layer of sp^2-bonded carbon, possesses several unique properties, including high thermal conductivity, high fracture strength, large specific surface area and extraordinary electronic transport property [22,23]. Economically, reduced graphene oxides (rGO) are usually derived from exfoliation of graphite oxide followed by reduction [24]. Compared with active carbon and multiwalled carbon nanotubes, graphene sheets have a higher surface to volume ratio owing to the accessibility of the inner surface, providing more available sites for the growth of nZVI particles. Moreover, the superior conductivity of rGO sheets offers efficient electron transfer between nZVI and targeted pollutants. For example, rGO-supported nZVI (nZVI@rGO) has been successfully prepared by Sun et al. [25] for the removal of U(VI) in solution. The incorporation of rGO can well disperse nZVI and clearly improve U(VI) removal reaction. Sahu et al. [26] have prepared the rGO supported bimetallic Fe/Ni nanocomposites. The microstructures as well as the electrochemical properties of the resulting rGO/Fe/Ni have been investigated to elucidate the dechlorination behavior toward trichloroethylene (TCE) under various conditions. TCE dechlorination efficiency of rGO/Fe/Ni nanocomposites is 2.4 times higher than that of free Fe/Ni nanoparticles, confirming the key role of rGO. Consequently, rGO sheets are a favorable alternative, compared with other carbon materials, in terms of supporting nZVI particles. However, the combination of nZVI and rGO is not sufficiently tight, which needed to be improved. To address this issue, Fe_3O_4 has been introduced by Lv et al. [27] as the middle layer between nZVI and rGO. The resulting nZVI particles are perfectly dispersed either among Fe_3O_4 particles or above the rGO-basal plane. In addition, Fe_3O_4 particles have attracted world-wide attention not only because of their unique size and morphology dependent physical or chemical properties but also for their biocompatibility and catalytic ability [28]. Furthermore, Fe_3O_4 particles could provide a convenient way for separating nanomaterials from treated water with the aid of an external magnetic field due to their magnetic nature [29]. Therefore, it could be supposed that assembling of nZVI on a magnetic Fe_3O_4/rGO composite could be rather beneficial for CL-20 reduction.

In this study, nZVI assembled on magnetic Fe_3O_4/rGO composite (nZVI@MG) was prepared for effective removal of CL-20 from synthetic wastewater. The performance of nZVI@MG in CL-20 removal was evaluated, compared with commercial ZVI powder, nZVI, MG and nZVI@rGO. The effects of operational conditions on CL-20 removal by nZVI@MG were investigated. In addition, possible CL-20 degradation pathways by nZVI@MG were proposed based on the identification of degradation intermediates.

2. Materials and methods

2.1. Preparation of GO and nZVI@rGO composites

GO was synthesized from graphite powder by a modified Hummers method [30]. Briefly, a three-neck flask was placed in an ice bath and the temperature carefully controlled to below 20°C and 46 mL of H_2SO_4 (98%) was added, followed by the addition of 1 g graphite, 1 g $NaNO_3$ and 4 g $KMnO_4$ under stirring for 30 min. The mixture was then stirred at room temperature for 1 h until its color turned to taupe brown and became pasty. Then, 60 mL of deionized water was slowly added under vigorous stirring and the diluted suspension was stirred at 90°C for 30 min. Finally, 140 mL of deionized water and 20 mL H_2O_2 (30%) were added and stirred for 30 min. For purification, the mixture was centrifuged and then washed with 30% HCl before washing

several times with deionized water. The obtained GO solid was dried under vacuum for 8 h for further usage.

To prepare nZVI@rGO, 0.1 g of GO prepared as above was exfoliated into 200 mL deionized water under ultrasound for 24 h. Then, the solution was transferred to a three-neck flask and purged with N_2 for 30 min to remove dissolved oxygen. Under stirring, 100 mL aqueous solution containing 2.48 g of $FeSO_4·7H_2O$ was slowing injected into the GO suspension. After mixing for 30 min, 100 mL of $NaBH_4$ solution (20 g/L) was added to the mixture drop by drop under N_2 protection. The products were collected by vacuum filtration and washed several times with deionized water and ethanol, before being dried under vacuum at 60°C. Finally, the obtained nZVI@rGO particles were stored in an N_2-purged desiccator. Ferrous iron (Fe^{2+}) was reduced by $NaBH_4$ according to the following reaction [31]:

$$Fe(H_2O)_6^{2+} + 2BH_4^- \rightarrow Fe^0 \downarrow + 2B(OH)_3 + 7H_2 \uparrow \qquad (1)$$
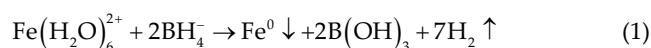
2.2. Preparation of MG and nZVI@MG composites

Before the synthesis of nZVI@MG, MG was prepared according to Ren et al. [32]. Briefly, the prepared GO (0.1 g) was exfoliated by ultrasonication in 80 mL of ethylene glycol (EG) for more than 24 h. Then, 1.8 g of $FeCl_3·6H_2O$ and 3.6 g of sodium acetate (NaAc) were dissolved in the GO-EG solution at ambient temperature. After stirring for ~30 min, the solution was transferred into a 100 mL Teflon-lined stainless steel autoclave and held at 200°C for 6 h before cooling naturally to ambient temperature. The obtained black MG was collected by filtration and washed with ethanol three times.

MG nanocomposites obtained above were rinsed several times with oxygen-free deionized water and then transferred into a three-neck flask. Next, 400 mL of oxygen-free deionized water was poured into this flask followed with addition of 2.48 g of $FeSO_4·7H_2O$ under vigorous stirring. Then, 50 mL of $NaBH_4$ solution (13.5 g/L) was added into the three-neck flask drop by drop to guarantee complete reaction. To remove residual impurities, the final product was washed with deionized water and ethanol three times. According to the above procedure, 1.071 g of nZVI@MG nanocomposite was synthesized at an $nZVI/Fe_3O_4/rGO$ mass ratio of 5/5/1.

2.3. CL-20 removal by nZVI@MG

In this study, a batch experiment was conducted to evaluate CL-20 removal by nZVI@MG, using 120 mL serum bottles containing 100 mL of synthetic wastewater as batch reactors. The reactors were placed on a rotary shaker at 200 rpm and 30°C for intensive mixing. The synthetic wastewater was prepared by dissolving 5 mg of CL-20 into 100 mL of acetonitrile aqueous solution (50%, v/v) and the final CL-20 concentration controlled at 50 mg/L. To maintain anaerobic conditions, the solution was purged with nitrogen gas for at least 10 min to remove residual dissolved oxygen. The serum bottles were immediately sealed with butyl rubber stoppers after the addition of iron composites. During the CL-20 removal process, 0.022 g of nZVI@MG was added into each serum bottle and reacted for 120 min. For comparison,

the CL-20 removal performance of commercial ZVI powder, nZVI, MG and nZVI@rGO was also evaluated. The dosages of ZVI powder, nZVI and nZVI@rGO were controlled at 0.01, 0.01 and 0.012 g, respectively, to ensure the same dosage of ZVI (0.01 g) as in 0.022 g of nZVI@MG. CL-20 removal by 0.012 g of MG was also investigated as the control. All batch experiments were performed at an initial pH of 3.0.

The effects of Fe_3O_4 dosage on CL-20 removal and nZVI@MG with different $nZVI/Fe_3O_4/rGO$ mass ratios (5/5/1, 5/3/1 and 5/1/1) were investigated by arranging different $FeCl_3·6H_2O$ dosages during MG preparation. However, with the ratio of $nZVI/Fe_3O_4/rGO$ varied, nZVI content was held at 0.10 g/L. The effects of nZVI@MG dosage on CL-20 removal were investigated at nZVI@MG dosage varied from 0.022 to 0.044 g. The effects of initial pH on the removal efficiency by nZVI@MG were tested with pH ranging from 3.0 to 7.0. The effects of NaCl concentration on the removal efficiency were also examined with NaCl concentrations ranged from 0 to 2,000 mg/L according to Lv et al. [33] but with slight modifications.

2.4. Analytical methods

Scanning electron microscopy (SEM; Quant™ 250 FEG, Thermo Fisher Scientific Inc., Waltham, MA, USA) and transmission electron microscopy (TEM; JEM 2100, JEOL Ltd., Tokyo, Japan) were used to characterize the surface morphology of nanocomposites, including bare rGO, nZVI, MG, nZVI@rGO and nZVI@MG. XRD analysis was carried out on a Bruker-AXSD8 system (Bruker Corp., Billerica, MA, USA) with Cu-K_α radiation source operating at 40 kV and 40 mA. FTIR spectroscopy (Nicolet iS10, Thermo Fisher Scientific Inc.) was used for the identification of the functional groups and composite chemical bonding within the wavenumber range of 4,000–400 cm^{-1}.

During the reaction process, 1 mL solution was withdrawn from serum bottles at desired time intervals and then filtered through a 0.22 µm membrane for further analysis. CL-20 was identified and quantified by high performance liquid chromatography (HPLC, LC-20AT, Shimadzu Corp., Kyoto, Japan) with a mobile phase of water/methanol (50/50, v/v), flowing at 1.0 mL min⁻¹ and the injection volume for all samples at 10 µL. An HPLC column (Inertsil® ODS-SP 5 µm, 25 cm × 4.6 mm, Shimadzu Corp.) was used for reversed-phase separation with column temperature of 40°C and detection at 223 nm for CL-20. All analyses were conducted in triplicate and the data were reported as the arithmetic mean ± standard deviation.

3. Results and discussion

3.1. Characterization of nZVI@MG particles

The morphologies of bare GO, nZVI@rGO and nZVI@MG nanocomposites were characterized by SEM and TEM. Bare GO and nZVI@rGO displayed clear differences with bare GO displaying a crumpled but clean paper-like structure, while a large number of granular particles were closely attached on rGO sheet surfaces, indicating the formation of loosely packed nZVI onto rGO (Fig. 1). Ma et al. [34] have found that nZVI particles show a tendency to conglutinate
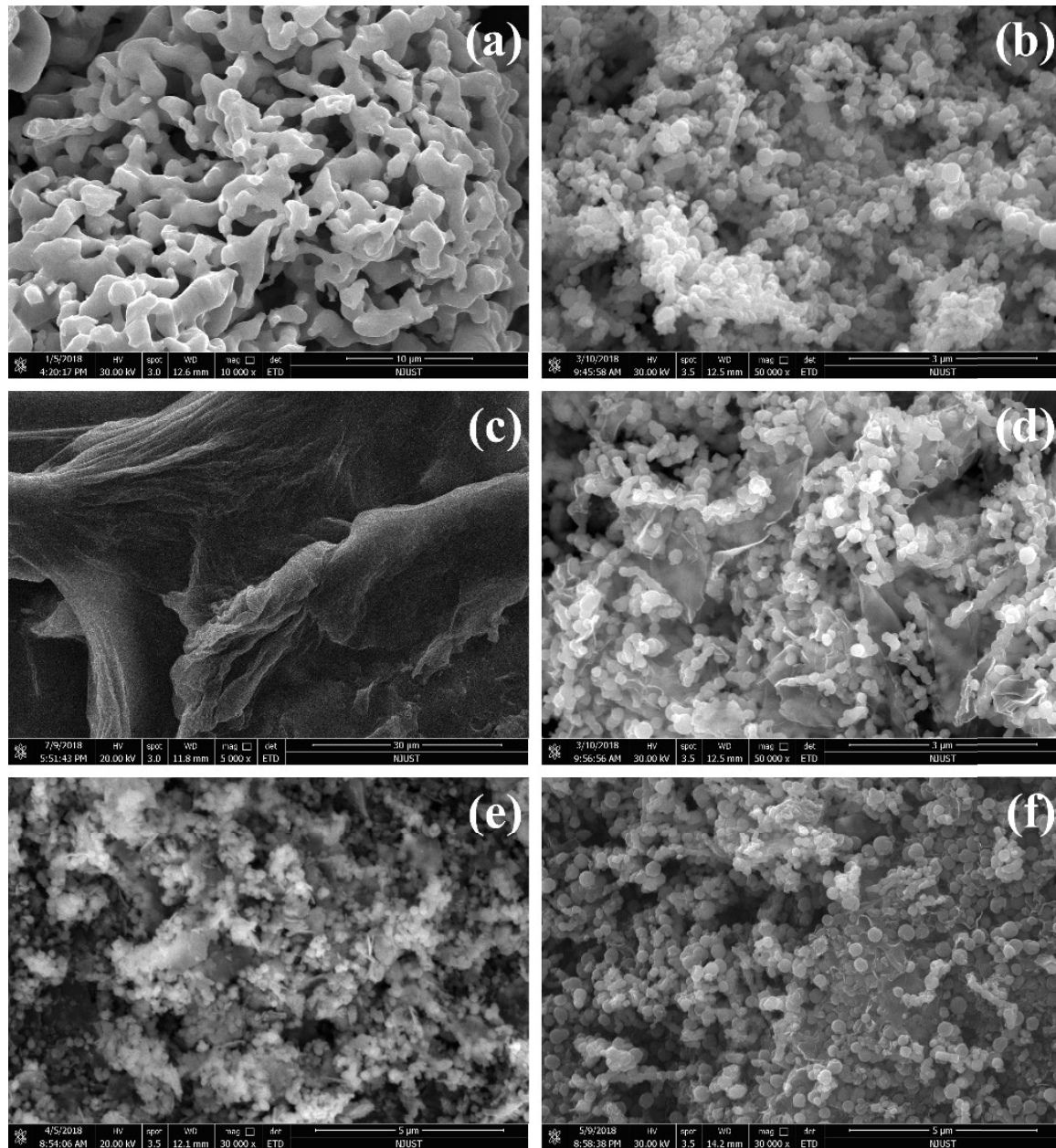
Fig. 1. SEM images of commercial ZVI (a), nano Fe_3O_4 (b) GO (c), nZVI@rGO (d), MG (e) and nZVI@MG (f).

one by one into branch-like forked chains and attach onto graphene sheet surfaces, which was also observed in this study (Fig. 1c). However, from the SEM image of nZVI@ MG, it was inferred that, with the integration of Fe_3O_4 as the middle layer, nZVI and rGO were combined more tightly. More evenly distributed nZVI chains on MG provided more activated sites and larger surface areas. From TEM images, it was observed that nZVI chains were assembled onto rGO basal planes (Fig. 2a). However, the black and spherical Fe_3O_4 nanoparticles, with average diameters of ~10–30 nm, were tightly attached to the graphene basal plane (Fig. 2b). The nZVI particles with average diameter of 40–200 nm were well embedded with Fe_3O_4 nanoparticles (Fig. 2b). A similar phenomenon has been observed by Lv et al. [27], where

nZVI showed good dispersion performance on Fe_3O_4/rGO composites. As it is rather critical to disperse nZVI particles uniformly and stably, the newly synthesized nZVI@ MG nanocomposites were expected to possess high activity toward CL-20.

According to XRD patterns, nZVI nanoparticles showed a markable peak at 2θ of 44.5° (Fig. 3). The typical peaks at 30.2°, 35.7°, 43.0°, 57.2° and 62.5° are assigned to (220), (311), (400), (511) and (440) reflected Fe_3O_4 crystal facet [35]. After coupling with graphene, typical peaks corresponding to nZVI and Fe_3O_4 nanoparticles were also observed for samples of nZVI@rGO and MG, indicating the successful loading of nZVI and Fe_3O_4 nanoparticles onto rGO. However, no significant peaks of graphene appeared that
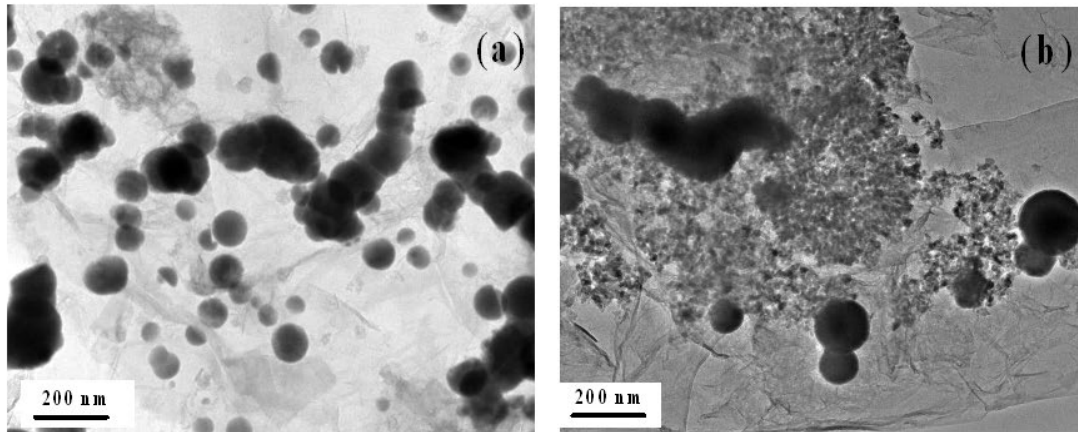
Fig. 2. TEM images of nZVI@rGO (a) and nZVI@MG (b).
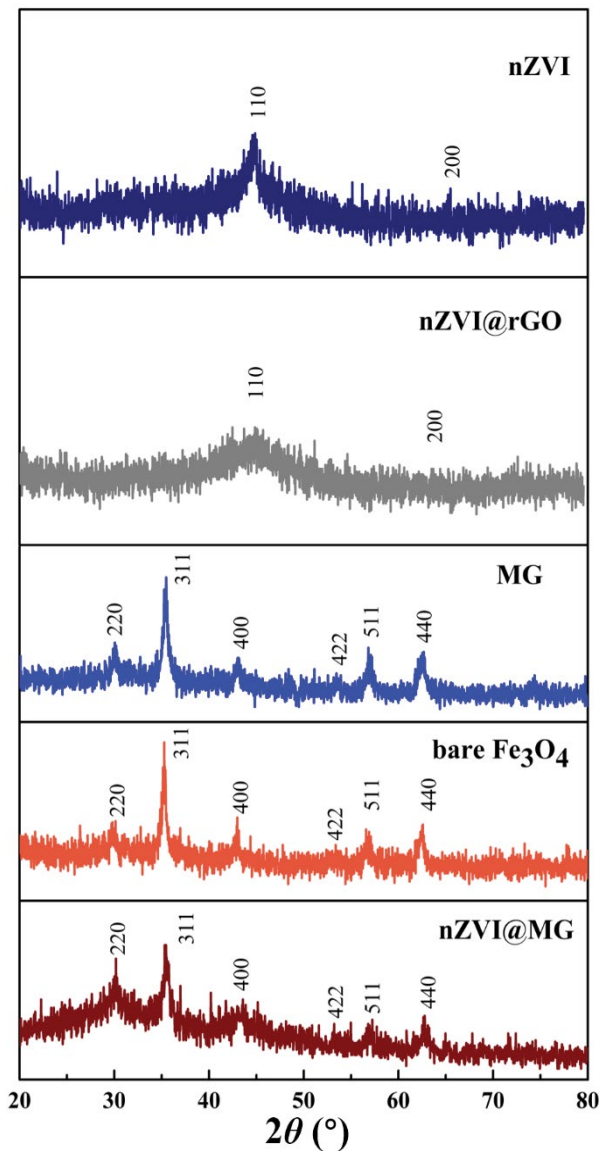
Fig. 3. XRD patterns of synthetic materials.

might have been due to more disordered stacking and less agglomeration of graphene in the composite [36]. For nZVI@MG composites, peaks corresponding to Fe_3O_4 nanoparticles were clearly observed. However, due to the low concentration of nZVI, only small and relatively wide diffraction peaks of nZVI were observed in the patterns of nZVI@MG, suggesting that nZVI constituents of nZVI@MG were in an amorphous state. This phenomenon has also been reported in the literature [37,38].

FTIR spectra showed that GO showed typical peaks related to different oxygen-containing functional groups (Fig. 4) [39,40]. For instance, carboxyl groups present at 1,410 and 1,720 cm^{-1} corresponded to C–OH and C=O stretching vibrations, respectively. Epoxy groups exhibited vibrational bands at 1,160 cm^{-1} that corresponded to the C–O–C breathing mode. After the introduction of Fe_3O_4 nanoparticles, several peaks at 1,100 and 600–700 cm^{-1} appeared, which were assigned to the Fe–O–Fe and Fe–O stretching vibrations of Fe_3O_4 nanoparticles [41]. After nZVI particles loading onto MG, the peak for Fe_3O_4 nanoparticles at 1,100 cm^{-1} was diminished while those at 600–700 cm^{-1} were enhanced, which was attributed to $NaBH_4$ reduction toward MG. These phenomena were consistent with a report by Lv et al. [27], confirming the successful synthesis of nZVI@MG.

3.2. Application of nZVI@MG for CL-20 removal

The CL-20 degradation performance of nZVI@MG was investigated and the results showed that bare MG exhibited slight removal toward CL-20, indicating that the CL-20 adsorption by MG was ignorable, probably due to the usage of acetonitrile as a solvent in synthetic wastewater (Fig. 5). After reaction for 120 min, CL-20 removal efficiency was as low as 27.9% ± 1.6% and 53.2% ± 0.9% which was achieved in the serum bottles dosed by commercial ZVI powder and nZVI, respectively. Improvement of CL-20 removal was observed in the reaction system supplemented by nZVI@rGO, confirming the stimulant role of rGO as a supporter for the nZVI loading. However, the best removal efficiency of CL-20 was obtained via the nZVI@MG treatment system, in which CL-20 was completely removed within 120 min. This is because of the synergetic effects between nZVI and
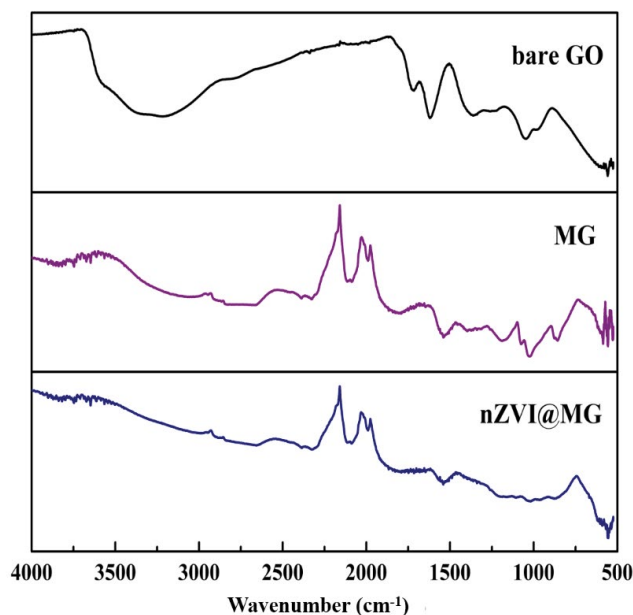
Fig. 4. FTIR spectrums for synthetic materials.
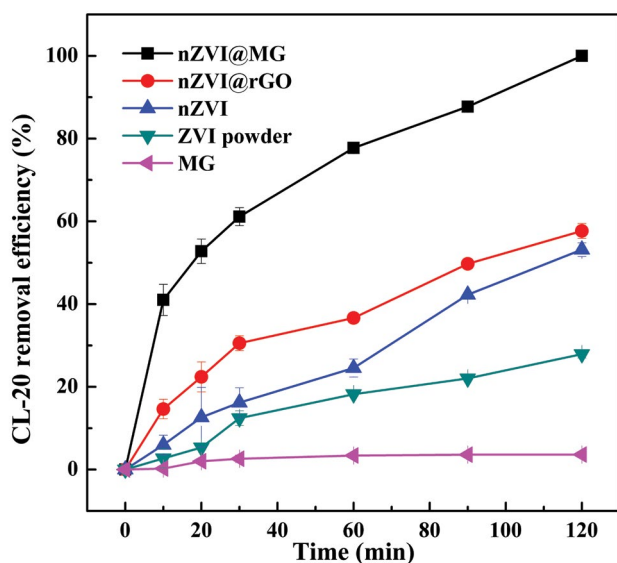
Fig. 5. Overall performance of blank MG, ZVI powder, nZVI, nZVI@rGO and nZVI@MG in terms of CL-20 removal.

rGO as well as the contribution of Fe_3O_4 as both conductor and binder. The Fe_3O_4 particles had a large surface area and an excellent electron transfer capacity that improved the dispersibility and reducibility of nZVI. During the electron transfer from nZVI to CL-20, Fe^{2+} and $Fe(OH)_2$ were formed and assisted CL-20 reduction [27]. However, the concentration of total Fe ions was not significant (~1.0–3.0 mg/L), suggesting that CL-20 reduction mainly occurred on the solid surface and not in the solution.

The important role of Fe_3O_4 nanoparticles was verified by investigating the CL-20 removal performance by nZVI@ MG with different mass ratios of $nZVI/Fe_3O_4$. As the nZVI/ Fe_3O_4 ratio increased from 5/1 to 5/5, CL-20 removal was significantly enhanced (Fig. 6a). CL-20 was completely removed within 120 min at an $nZVI/Fe_3O_4$ mass ratio of 5/5, while only 69.2% ± 1.3% CL-20 was removed by nZVI@MG with an $nZVI/Fe_3O_4$ ratio of 5/1. It was inferred that a high Fe_3O_4 content in nZVI@MG composites corresponded to an improved CL-20 removal efficiency. On the one hand, Fe_3O_4 processed certain adsorption capacity to CL-20, which promoted CL-20 reduction by nZVI@MG. On the other hand, the presence of Fe_3O_4 accelerated electron transfer from nZVI to the Fe^{3+} of Fe_3O_4, which enhanced nZVI corrosion and produced more Fe^{2+} for CL-20 reduction [42].

The nZVI@MG dosage is rather crucial for CL-20 removal. The influence of nZVI@MG dosage (0.22–0.44 g/L) on CL-20 removal was determined and the CL-20 removal efficiencies shown in Fig. 6b. With increased nZVI@MG dosage, both the total amount and total surface area of nZVI was involved in the reaction increase, which provided more free electrons for the reductive degradation. As a result, the time required for complete removal of CL-20 clearly shortened from 120 to 60 min. Li et al. [43] have indicated that the reaction rate of Cr(VI) is effectively promoted with increased nZVI dosage, which was here attributed to increased adsorption and reaction sites.

Solution pH is always a predominating factor affecting the existing species forms and uptake behavior of adsorbents [38]. The effects of pH during CL-20 removal were investigated by testing the CL-20 removal under different initial pH conditions. As the initial pH value decreased from 7.0 to 3.0, CL-20 removal efficiency increased slightly from 85.5% ± 0.5% to 100%. Lv et al. [42] have found that nZVI nanoparticles always showed better removal efficiency in an acid environment, which was consistent with this study. At higher pH, generated ferric hydroxide attached to nZVI@ MG surfaces and increased the reaction efficiency. In contrast, acidic conditions accelerated the dissolution of iron oxide formed on nZVI@MG surfaces, resulting in more active sites for CL-20 removal. However, it was clearly observed that nZVI@MG degraded CL-20 efficiently even at a neutral pH of 7.0, indicating excellent reductive performance by nZVI@MG.

For the reduction of various pollutants, such as CL-20, electrolytes, such as NaCl, play a key role in electron transfer [44]. As NaCl concentration increased from 0 to 2,000 mg/L, CL-20 removal efficiency by nZVI@MG within 90 min increased from 87.7% ± 0.5% to 94.7% ± 1.1%. (Fig. 6d). CL-20 removal was enhanced by Cl^-, which tended to accelerate the iron corrosion by aggressively diffusing into passivated oxides and forming strong complexes with iron centers [45]. It should be noted, however, that the promotive role of the electrolyte was very limited due to the superiority of nZVI@ MG, as indicated by the minor effects of NaCl concentration toward CL-20 removal.

3.3. CL-20 removal kinetics

According to the literature, nitroaromatic compounds removal by nZVI-based materials often undergoes a multi-step process that involves electrostatic adsorption and subsequent reduction [46]. To understand the adsorption in detail, both a pseudo-first-order reaction model and pseudo-second-order
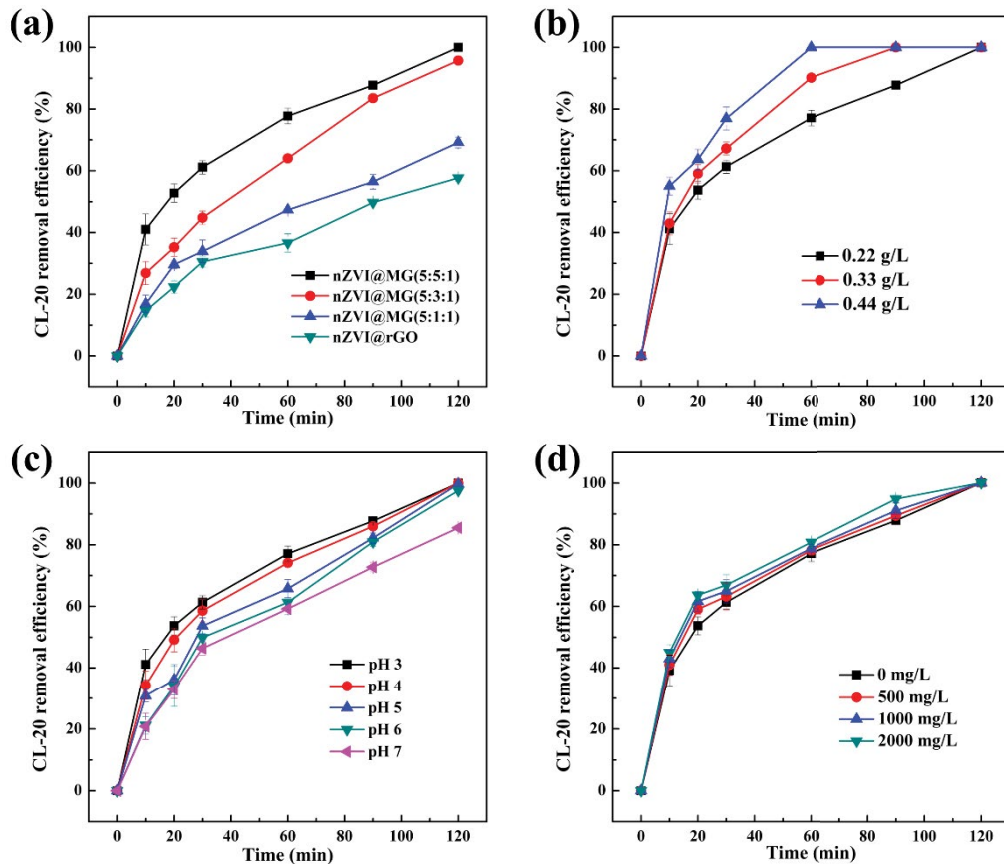
Fig. 6. CL-20 removal by nZVI@MG at different nZVI/Fe$_3$O$_4$ ratio of nZVI@MG (a), at different amount of nZVI@MG (b), at different pH values (c) and at different NaCl concentration (d).

adsorption model were investigated to describe the adsorption process [47], which were expressed by the following equations.

Pseudo-first-order reaction model

$$\ln\left(q_e - q_t\right) = \ln\left(q_e\right) - k_1 t \tag{2}$$

Pseudo-first-order reaction model

$$\frac{t}{q_t} = \frac{1}{k_2 q_e^2} + \frac{t}{q_e} \tag{3}$$

where q_t and q_e represent the amounts of CL-20 adsorbed onto adsorbents at any time t or at equilibrium time (mg g^{-1}), respectively, and k_1 (min^{-1}) and k_2 (mg g^{-1} min^{-1}) represent the kinetic rate constants, respectively. A pseudo-second-order reaction model appeared to be more suitable for the description of CL-20 removal profile by nZVI@MG, as indicated by the coefficient R^2 as high as 0.9945 (Fig. 7). However, the correlation coefficients of the pseudo-first-order reaction model was relatively lower (R^2 = 0.9719), which revealed that the main CL-20 adsorption mechanism on the surface of nZVI@MG composites was chemical adsorption. Wu et al. [48] have also found that the removal of para-nitrochlorobenzene by nZVI followed a pseudo-second-order adsorption model, indicating that adsorption could probably be the

rate controlling step of the entire process. In addition, for the CL-20 removal profile by MG, the pseudo-second-order adsorption model fit the data very well (R^2 > 0.99). In general, the smaller the k_2 value, the higher the sorption rate [49]. In this study, the k_2 value for nZVI@MG was 12.0 times lower than that of MG, confirming that sorption rate of nZVI@MG was much higher than that of MG (Table 1). The equilibrium adsorption capacity (q_e) evaluated from the plot was found to be 238.10 mg g^{-1}, suggesting that the nZVI@MG system would be a good adsorbent for CL-20 removal from contaminated water. In previous experiments, bare MG could remove only 5% of CL-20 with 120 min, which indicated the potential adsorption capacity of MG. After nZVI@MG was added into CL-20 solution, CL-20 was first adsorbed onto nZVI@MG surfaces. After being reduced into new products, some were released back to the solution, with nZVI@MG surfaces regenerated for the further reduction reaction. Therefore, fast removal was observed at the initial stage, with relatively slow increases after 10 min.

3.4. Intermediates identification and CL-20 degradation pathways

During CL-20 removal by nZVI@MG, the degradation intermediates were detected by LC-MS or GC-MS (Table 2). LC-MS analysis showed the presence of intermediate IV at a retention time of 3.901 min (Fig. 8a), which showed [M – H]$^-$ ions at 385 Da. Intermediate VIII was detected with retention

D. Zhang et al. / Desalination and Water Treatment 182 (2020) 225–236
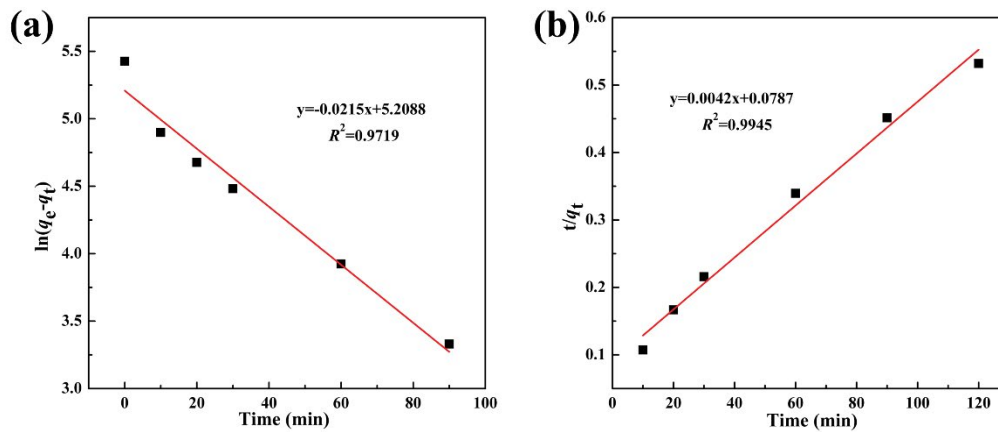
Fig. 7. CL-20 removal kinetics model.

Table 1
Pseudo-first-order kinetics and pseudo-second-order kinetics model for CL-20 removal on blank MG and nZVI@MG

Model	Parameters	MG	nZVI@MG
Pseudo-first-order kinetics	$q_{e(cal)}$ (mg g^{-1})	18.90	182.87
	$q_{e(exp)}$ (mg g^{-1})	18.36	227.27
	k_1 (min^{-1})	0.0301	0.0215
	R^2	0.9217	0.9719
Pseudo-second-order kinetics	$q_{e(cal)}$ (mg g^{-1})	18.56	238.10
	$q_{e(exp)}$ (mg g^{-1})	18.36	227.27
	k_2 (g mg^{-1} min^{-1})	2.91×10^{-3}	2.24×10^{-4}
	R^2	0.9936	0.9945

Table 2
Intermediates during CL-20 degradation identified by (a) LC-MS (b) GC-MS

Compound number	Chemical structure	Molecular formula	Retention time(min)	m/z
CL-20		$C_6H_6N_{12}O_{12}$	12.717 min[a]	438
IV		$C_6H_{10}N_{10}O_6$	3.901 min[a]	386
VII		$C_6H_{10}N_{12}O_8$	29.492 min[b]	378
VIII		$C_6H_{18}N_{12}O_4$	1.78 min[a]	322

times of 1.78 min (Figs. 8b and c) and showed $[M - H]^-$ at 321 Da and $[M + H]^+$ at 323 Da. Another intermediate VII was identified through GC-MS analysis (Fig. 8d), based on its most abundant fragments found at $m/z = 378$ [M+].

Based on the analysis of the above intermediates, two possible CL-20 degradation pathways were proposed (Fig. 9). In the first pathway, the elongated C–C bond at the molecule top was the weakest bond and cleaved first and then Intermediates II and III, which were observed during biodegradation [50], photodenitration [10] and ZVI reduction [11], were generated. Imine II was readily hydrated in water [51] and formed the hydroxyl nitramine (III). The
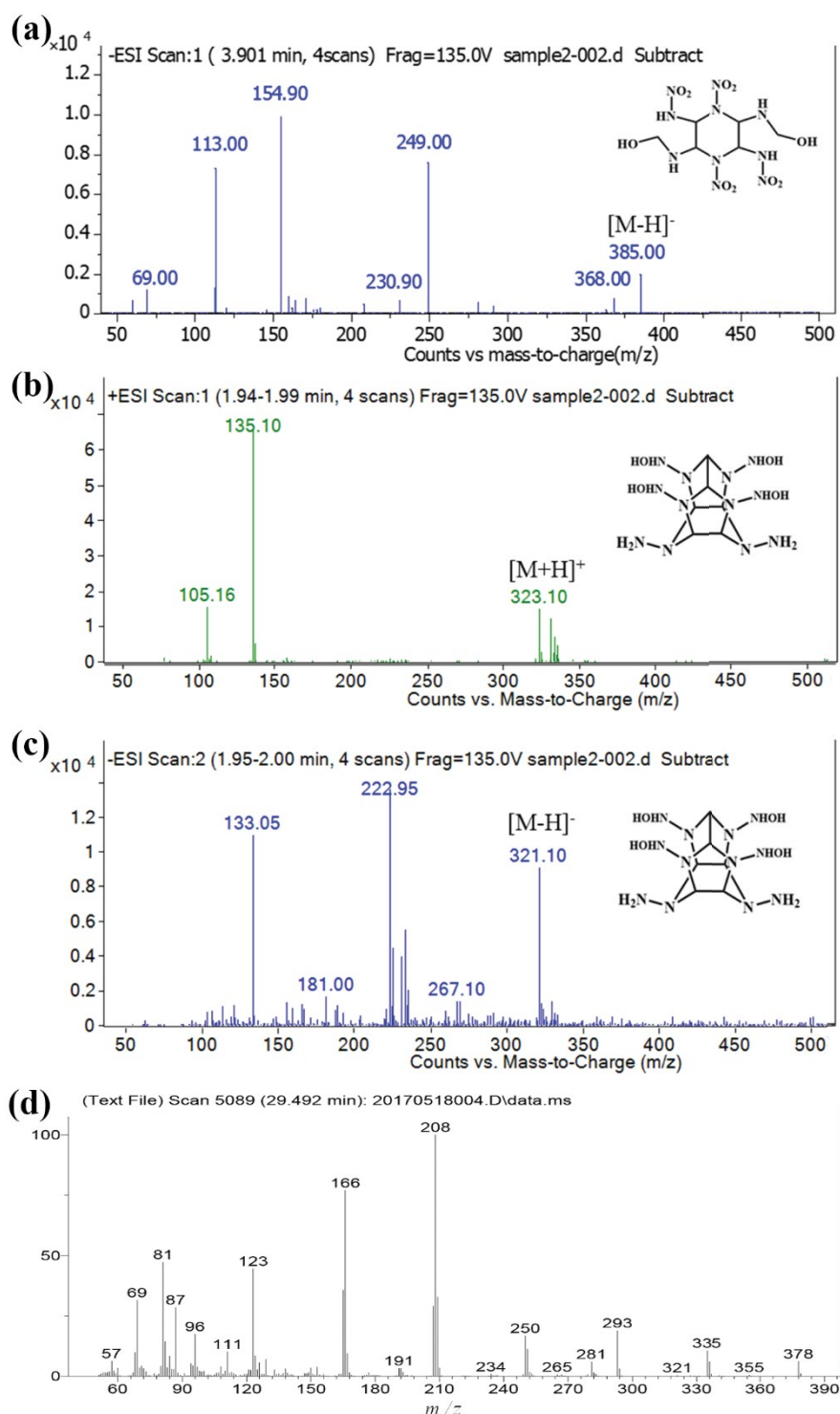
Fig. 8. LC-MS (a, b and c) and GC-MS (d) analysis of intermediates during CL-20 degradation by nZVI@MG.
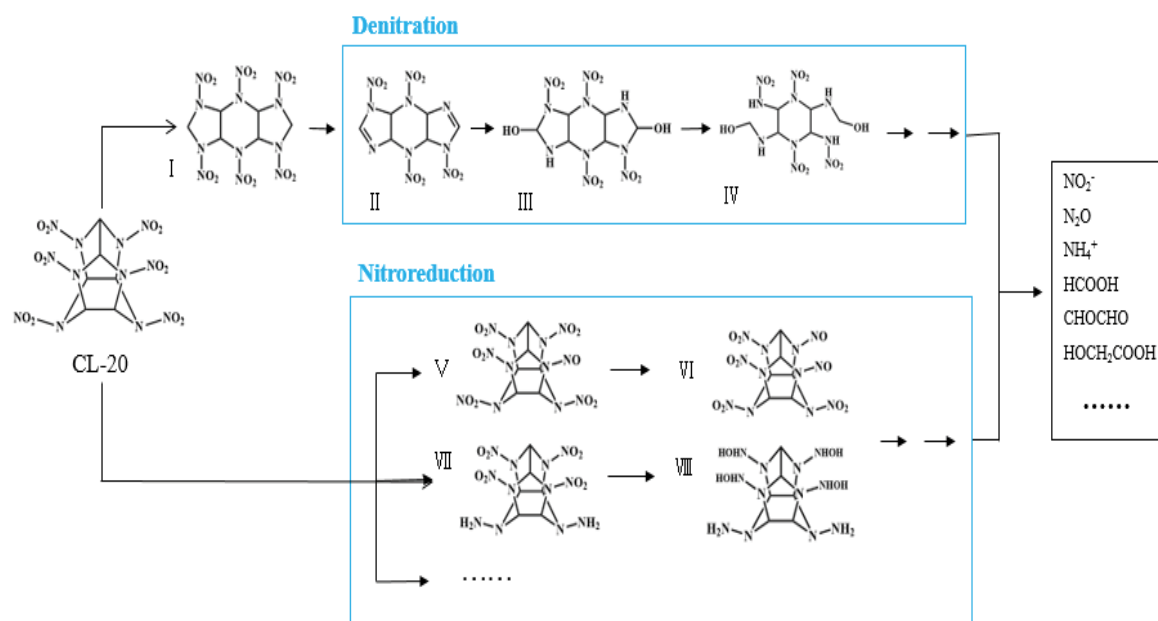
Fig. 9. Proposed CL-20 degradation pathways by nZVI@MG.

resulting hydroxyl nitramines were unstable and expected to undergo a rapid ring cleavage (across the $O_2NN–COH$ bond). This cleavage ultimately produced formate from the elongated C–C bond and glyoxal from the remaining two C–C bonds in CL-20, with the formation of product IV at the same time. Intermediates VI to VIII indicated a second pathway for CL-20 degradation. Nitroso products of CL-20 have also been reported in previous studies [11]. Therefore, the sequential reduction of $N–NO_2$ groups to the corresponding $N–NH_2$ derivatives was demonstrated here to be a great possibility. $N–NO_2$ reduction underwent a sequential process of $N–NO_2$, N–NO, N–NHOH, $N–NH_2$ and N–NO, which have been as detected in previous studies, therefore the presenting intermediates VII and VIII as the possibilities of a nitroreduction pathway.

4. Conclusions

In the present study, a highly efficient reductant was successfully synthesized by loading nZVI composite onto MG. CL-20 removal by nZVI@MG was significantly enhanced, compared with ZVI powder, nZVI, nZVI@rGO and blank MG. CL-20 removal by nZVI@MG followed a pseudo-second-order kinetics model, indicating the involvement of a hybrid chemical reaction–adsorption process. A synergistic mechanism, including chemical adsorption of CL-20 onto nZVI@MG, direct reduction by nZVI and enhanced electron transfer by rGO and Fe_3O_4, was responsible for the enhanced CL-20 removal by nZVI@MG. The excellent reducibility of nZVI@MG yielded it a promising alternative for the remediation of CL-20 contaminated waters. Through LC-MS and GC-MS analysis, three new intermediates were detected and two degradation pathways were proposed, including denitration and nitroreduction.

References

[1] Y. Kholod, S. Okovytyy, G. Kuramshina, M. Qasim, L. Gorb, J. Leszczynski, An analysis of stable forms of CL-20: a DFT study of conformational transitions, infrared and Raman spectra, J. Mol. Struct., 843 (2007) 14–25.

[2] R.L. Simpson, P.A. Urtiew, D.L. Ornellas, G.L. Moody, K.J. Scribner, D.M. Hoffman, CL-20 performance exceeds that of HMX and its sensitivity is moderate, Propell. Explos. Pyrot., 22 (1997) 249–255.

[3] P.Y. Robidoux, G.I. Sunahara, K. Savard, Y. Berthelot, F. Leduc, S. Dodard, M. Martel, P. Gong, J. Hawari, Acute and chronic toxicity of the new explosive CL-20 to the earthworm (*Eisenia andrei*) exposed to amended natural soils, Environ. Toxicol. Chem., 23 (2004) 1026–1034.

[4] S. Dodard, G.I. Sunahara, M. Sarrazin, P. Gong, R.G. Kuperman, G. Ampleman, S. Thiboutot, J. Hawari, Survival and reproduction of enchytraeid worms (*Oligochaeta*) in different soil types amended with cyclic nitramine explosives, Environ. Toxicol. Chem., 24 (2005) 2579–2587.

[5] R.G. Kuperman, R.T. Checkai, M. Simini, C.T. Phillips, J.S. Anthony, J.E. Kolakowski, E.A. Davis, Toxicity of emerging energetic soil contaminant CL-20 to potworm *Enchytraeus crypticus* in freshly amended or weathered and aged treatments, Chemosphere, 62 (2006) 1282–1293.

[6] J.C. Pennington, J.M. Brannon, Environmental fate of explosives, Thermochim. Acta, 384 (2002)163–172.

[7] S. Trott, S.F. Nishino, J. Hawari, J.C. Spain, Biodegradation of the nitramine explosive CL-20, Appl. Environ. Microbiol., 69 (2003) 1871–1874.

[8] P. Karakaya, M. Sidhoum, C. Christodoulatos, S. Nicolich, W. Balas, Aqueous solubility and alkaline hydrolysis of the

novel high explosive hexanitrohexaazaisowurtzitane (CL-20), J. Hazard. Mater., 120 (2005) 183–191.

[9] V.K. Balakrishnan, A. Halasz, J. Hawari, Alkaline hydrolysis of the cyclic, nitramine explosives RDX, HMX, and CL-20: new insights into degradation pathways obtained by the observation of novel intermediates, Environ. Sci. Technol., 37 (2003) 1838–1843.

[10] J. Hawari, S. Deschamps, C. Beaulieu, L. Paquet, A. Halasz, Photodegradation of CL-20: Insights into the mechanisms of initial reactions and environmental fate, Water Res., 38 (2004) 4055–4064.

[11] V.K. Balakrishnan, F. Monteil-Rivera, A. Halasz, A. Corbeanu, J. Hawari, Decomposition of the polycyclic nitramine explosive, CL-20, by Fe, Environ. Sci. Technol., 38 (2004) 6861–6866.

[12] B.T. Oh, P.J.J. Alvarez, Hexahydro-1,3,5-Trinitro-1,3,5-Triazine (Rdx) degradation in biologically-active iron columns, Water Air Soil Pollut., 141 (2002) 325–335.

[13] W. Jiamjitrpanich, C. Polprasert, P. Parkpian, R.D. Delaune, A. Jugsujinda, Environmental factors influencing remediation of TNT-contaminated water and soil with nanoscale zero-valent iron particles, J. Environ. Sci. Health, 45 (2010) 263–274.

[14] X. Zhang, S. Lin, Z.L. Chen, M. Megharaj, R. Naidu, Kaolinite-supported nanoscale zero-valent iron for removal of Pb^{2+} from aqueous solution: reactivity, characterization and mechanism, Water Res., 45 (2011) 3481–3488.

[15] N.C. Mueller, J. Braun, J. Bruns, M. Cernik, P. Rissing, D. Rickerby, B. Nowack, Application of nanoscale zero valent iron (NZVI) for groundwater remediation in Europe, Environ. Sci. Pollut. Res., 19 (2012) 550–558.

[16] Q. Huang, S. Song, Z. Chen, B.W. Hu, J.R. Chen, X.K. Wang, Biochar-based materials and their applications in removal of organic contaminants from wastewater: state-of-the-art review, Biochar, 1 (2019) 45–73.

[17] X.X. Wang, L. Chen, L. Wang, Q.H. Fan, D.Q. Pan, J.X. Li, F.T. Chi, Y.X. Xie, S.J. Yun, C.L. Xiao, F. Luo, J. Wang, X.L. Wang, Synthesis of novel nanomaterials and their application in efficient removal of radionuclides, Sci. China Chem., 62 (2019) 933–967.

[18] H.J. Zhu, Y.F. Jia, X. Wu, H. Wang, Removal of arsenic from water by supported nano zero-valent iron on activated carbon, J. Hazard. Mater., 72 (2009) 1591–1596.

[19] X.S. Lv, J. Xu, G.M. Jiang, X.H. Xu, Removal of chromium(VI) from wastewater by nanoscale zero-valent iron particles supported on multiwalled carbon nanotubes, Chemosphere, 85 (2011) 1204–1209.

[20] Z. Jiang, L. Lv, W.M. Zhang, Q. Du, B.C. Pan, L. Yang, Q.X. Zhang, Nitrate reduction using nanosized zero-valent iron supported by polystyrene resins: role of surface functional groups, Water Res., 45 (2011) 2196–2198.

[21] Z.X. Chen, X.Y. Jin, Z. Chen, M. Megharaj, R. Naidu, Removal of methyl orange from aqueous solution using bentonite-supported nanoscale zero-valent iron, J. Colloid Interface Sci., 363 (2011) 601–607.

[22] X.L. Liu, R. Ma, X.X. Wang, Y. Ma, Y.P. Yang, L. Zhang, S. Zhang, R. Jehan, J.R. Chen, X.K. Wang, Graphene oxide-based materials for efficient removal of heavy metal ions from aqueous solution: a review, Environ. Pollut., 252 (2019) 62–73.

[23] X.H. Jia, H.J. Song, C.Y. Min, X.Q. Zhang, One-step synthesis of Fe_3O_4 nanorods/graphene nanocomposites, Appl. Phys. A, 109 (2012) 261–265.

[24] J.P. Rourke, P.A. Pandey, J.J. Moore, M. Bates, I.A. Kinloch, R.J. Young, N.R. Wilson, The real graphene oxide revealed: stripping the oxidative debris from the graphene-like sheets, Angew. Chem. Int. Ed. Engl., 50 (2011) 3173–3177.

[25] Y.B. Sun, C.C. Ding, W.C. Cheng, X.K. Wang, Simultaneous adsorption and reduction of U(VI) on reduced graphene oxide-supported nanoscale zerovalent iron, J. Hazard. Mater., 280 (2014) 399–408.

[26] R.S. Sahu, D.L. Li, R.A. Doong, Unveiling the hydrode-chlorination of trichloroethylene by reduced graphene oxide supported bimetallic Fe/Ni nanoparticles, Chem. Eng. J., 334 (2017) 30–40.

[27] X.S. Lv, X.Q. Xue, G.M. Jiang, D.L. Wu, T.T. Sheng, H.Y. Zhou, X.H. Xu, Nanoscale zero-valent iron (nZVI) assembled on magnetic Fe_3O_4/graphene for Chromium(VI) removal from aqueous solution, J. Colliod Interface Sci., 417 (2014) 51–59.

[28] L.H. Zhang, J.J. Wu, H.B. Liao, Y.L. Hou, S. Gao, Octahedral Fe_3O_4 nanoparticles and their assembled structures, Chem. Commun., 29 (2009) 4378–4380.

[29] L.L. Fan, C.N. Luo, X.J. Li, F.G. Lu, H.M. Qiu, M. Sun, Fabrication of novel magnetic chitosan grafted with graphene oxide to enhance adsorption properties for methyl blue, J. Hazard. Mater., 215–216 (2012) 272–279.

[30] W.S. Hummers, R.E. Offeman, Preparation of Graphitic Oxide, J. Am. Chem. Soc., 80 (1958) 1339–1339.

[31] C.B. Wang, W.X. Zhang, Synthesizing nanoscale iron particles for rapid and complete dechlorination of TCE and PCBs, Environ. Sci. Technol., 31 (1997) 2154–2156.

[32] L.L. Ren, S. Huang, W. Fan, T.X. Liu, One-step preparation of hierarchical superparamagnetic iron oxide/graphene composites via hydrothermal method, Appl. Surf. Sci., 258 (2011) 1132–1138.

[33] X.S. Lv, Y.J. Hu, J. Tang, T.T. Sheng, G.M. Jiang, X.H. Xu, Effects of co-existing ions and natural organic matter on removal of chromium (VI) from aqueous solution by nanoscale zero valent iron (nZVI)-Fe_3O_4 nanocomposites, Chem. Eng. J., 218 (2013) 55–64.

[34] Y.Y. Ma, X.F. Lv, Q. Yang, Y.Y. Wang, X. Chen, Reduction of carbon tetrachloride by nanoscale palladized zero-valent iron@ graphene composites: kinetics, activation en/ergy, effects of reaction conditions and degradation mechanism, Appl. Catal. A, 542 (2017) 252–261.

[35] X. Sun, Y.B. Yan, J.S. Li, W.Q. Han, L.J. Wang, SBA-15-incorporated nanoscale zero-valent iron particles for chromium(VI) removal from groundwater: mechanism, effect of pH, humic acid and sustained reactivity, J. Hazard. Mater., 266 (2014) 26–33.

[36] Z.S. Wu, W.C. Ren, L. Wen, L.B. Gao, J.P. Zhao, Z.P. Chen, G.M. Zhou, F. Li, H.M. Cheng, Graphene anchored with Co_3O_4 nanoparticles as anode of lithium ion batteries with enhanced reversible capacity and cyclic performance, ACS Nano, 4 (2012) 3187–3194.

[37] G.Z. Qu, D.Y. Zeng, R.J. Chu, T.C. Wang, D.L. Liang, H. Qiang, Magnetic Fe_3O_4 assembled on nZVI supported on activated carbon fiber for Cr(VI) and Cu(II) removal from aqueous solution through a permeable reactive column, Environ. Sci. Pollut. Res., 26 (2019) 5176–5188.

[38] X.F. Lv, H. Li, Y.Y. Ma, H. Yang, Q. Yang, Degradation of carbon tetrachloride by nanoscale zero-valent iron@magnetic Fe_3O_4: Impact of reaction condition, kinetics, thermodynamics and mechanism, Appl. Organomet. Chem., 32 (2018) 4139–4151.

[39] L.M. Pastrana-Martínez, S. Morales-Torres, V. Likodimos, P. Falaras, J.L. Figueiredo, J.L. Faria, A.M.T. Silva, Role of oxygen functionalities on the synthesis of photocatalytically active graphene-TiO_2 composites, Appl. Catal., B, 158–159 (2014) 329–340.

[40] M. Acik, G. Lee, C. Mattevi, A. Pirkle, R.M. Wallace, M. Chhowalla, K. Cho, Y. Chabal, The role of oxygen during thermal reduction of graphene oxide studied by infrared absorption spectroscopy, J. Phys. Chem. C, 115 (2015) 19761–19781.

[41] K. Yang, H.B. Peng, Y.H. Wen, N. Li, Re-examination of characteristic FTIR spectrum of secondary layer in bilayer oleic acid-coated Fe_3O_4 nanoparticles, Appl. Surf. Sci., 256 (2010) 3093–3097.

[42] X.S. Lv, J. Xu, G.M. Jiang, J. Tang, X.H. Xu, Highly active nanoscale zero-valent iron (nZVI)-Fe_3O_4 nanocomposites for the removal of chromium(VI) from aqueous solutions, J. Colloid. Interface Sci., 369 (2012) 460–469.

[43] X.Y. Li, L.H. Ai, J. Jiang, Nanoscale zerovalent iron decorated on graphene nanosheets for Cr(VI) removal from aqueous solution: Surface corrosion retard induced the enhanced performance, Chem. Eng. J., 288 (2016) 789–797.

[44] C.C. Xu, R. Liu, L.J. Chen, J.L. Tang, Enhanced dechlorination of 2,4-dichlorophenol by recoverable Ni-Fe-Fe_3O_4 nanocomposites, J. Environ. Sci., 48 (2016) 92–101.

[45] W.Z. Yin, J.H. Wu, P. Li, X.D. Wang, N.W. Zhu, P.X. Wu, Experimental study of zero-valent iron induced nitrobenzene

reduction in groundwater: the effects of pH, iron dosage, oxygen and common dissolved anions, Chem. Eng. J., 184 (2012) 198–204.

[46] W. Chen, P. Westerhoff, J.A. Leenheer, K. Booksh, Fluorescence excitation-emission matrix regional integration to quantify spectra for dissolved organic matter, Environ. Sci. Technol., 37 (2003) 5701–5710.

[47] M. Iram, C. Guo, Y. Guan, A. Ishfaq, H. Liu, Adsorption and magnetic removal of neutral red dye from aqueous solution using Fe_3O_4 hollow nanospheres, J. Hazard. Mater., 181 (2010) 1039–1050.

[48] Y. Wu, H. Luo, H. Wang, Removal of para-nitrochlorobenzene from aqueous solution on surfactant-modified nanoscale zero-valent iron/graphene nanocomposites, Environ. Technol., 35 (2014) 2698–2707.

[49] S.M. Maliyekkal, A.K. Sharma, L. Philip, Manganese-oxide-coated alumina: a promising sorbent for defluoridation of water, Water Res., 40 (2006) 3497–3506.

[50] B. Bhushan, L. Paquet, J.C. Spain, Biotransformation of 2,4,6,8,10,12-hexanitro-2,4,6,8,10,12-hexaazaisowurtzitane (CL-20) by denitrifying *Pseudomonas* sp. strain FA 1, J. Hawari Appl. Environ. Microbiol., 69 (2003) 5216–5221.

[51] J. March, Advanced Organic Chemistry, 3rd ed. Wiley-Interscience, New York, 1985, pp. 784–785.